



ELSEVIER

Nuclear Physics A579 (1994) 493–517

NUCLEAR  
PHYSICS A

## Spectral function of finite nuclei and scattering of GeV electrons

O. Benhar <sup>a</sup>, A. Fabrocini <sup>b</sup>, S. Fantoni <sup>c</sup>, I. Sick <sup>d</sup><sup>a</sup> INFN, Sezione Sanità, Physics Laboratory, Istituto Superiore di Sanità, I-00161, Rome, Italy<sup>b</sup> Department of Physics, University of Pisa, INFN, Sezione di Pisa, I-56100 Pisa, Italy<sup>c</sup> Interdisciplinary Laboratory, SISSA, INFN, Sezione di Trieste, I-34014 Trieste, Italy<sup>d</sup> Institut für Physik, Universität Basel, CH-4056 Basel, Switzerland

Received 9 February 1994; revised 9 May 1994

---

### Abstract

We employ the local-density approximation to derive the spectral function  $P(\mathbf{k}, E)$  of finite nuclei. For various densities of nuclear matter we calculate  $P(\mathbf{k}, E)$ , and split it into the single-particle and correlated parts. For *finite nuclei*  $P(\mathbf{k}, E)$  is calculated by combining the nuclear-matter correlated part, evaluated in local-density approximation, with the finite-nucleus single-particle part obtained from mean-field calculations or (e, e'p) experiments. These spectral functions are used to calculate cross sections for inclusive electron–nucleus scattering at large momentum transfer. The recoil-nucleon final-state interaction is treated in the local-density approximation as well.

**Keywords:** Nuclear structure; Spectral function of finite nuclei; Cross sections for inclusive electron scattering

---

### 1. Introduction

The knowledge of the spectral function  $P(\mathbf{k}, E)$ , the quantity that gives the probability to find in a nucleus a nucleon of momentum  $\mathbf{k}$  and removal energy  $E$ , is needed for the theoretical description of a number of nuclear processes. For the calculation of many observables it is important to have nuclear wave functions and spectral functions that are realistic for *both* the single-particle aspects *and* the short-range properties resulting from NN correlations.

The need for a realistic  $P(\mathbf{k}, E)$  is obvious in particular for processes involving large momentum transfers  $q$ . Examples for such processes are electron–nucleus scattering, be it in the regime of low energy transfer  $\omega$  of interest to quasi-elastic

scattering, or be it in the region of large  $\omega$  of interest for the understanding of deep inelastic scattering (EMC effect). In the kinematical region corresponding to low  $\omega$  and large momentum transfer  $q$ , where the impulse approximation is applicable, electron–nucleus scattering essentially reduces to the incoherent sum of elementary scattering processes on a collection of  $A$  off-shell nucleons distributed according to the spectral function  $P(\mathbf{k}, E)$ , which contains all the information on the structure of the nuclear target. The behaviour of  $P(\mathbf{k}, E)$  at large values of  $\mathbf{k}$  and  $E$  is of particular relevance for these applications, since at high  $q$  the electrons probe the short-range interparticle correlations, which are known to give rise to the high-momentum components in the nuclear wave functions.

Microscopic calculations of  $P(\mathbf{k}, E)$  based on realistic nuclear hamiltonians have been carried out for light nuclei with  $A \leq 4$ . The deuteron spectral function can be readily expressed in terms of the wave function in momentum space, whereas for the three-body systems  $P(\mathbf{k}, E)$  has been obtained both using the solution of the Faddeev equation [1,2] and within a variational approach [3]. The spectral function of the four-body nucleus  ${}^4\text{He}$  has been studied in Ref. [4] within the so-called ATMS approach, and in Refs. [5,6] using an approximate method based on the use of the microscopic momentum distribution of nucleons, deuterons,  ${}^3\text{H}$  and  ${}^3\text{He}$  in  ${}^4\text{He}$ . Applications to inclusive  $(e, e')$  scattering are discussed in Refs. [7,8,6].

Realistic many-body calculations have recently been extended [9] to obtain the momentum distribution  $n(\mathbf{k})$ , but not yet  $P(\mathbf{k}, E)$ , for  $A = 16$ , whereas for larger  $A$  one has to rely increasingly on more approximate treatments of nuclear structure. For heavy nuclei, reliable calculations of ground-state properties are available only within the mean-field framework and extensions thereof, approximations which are known to be inadequate to describe the high-momentum components of the nuclear wave functions.

Besides light nuclei, the only other system for which accurate microscopic calculations of the spectral function, starting from the NN interaction, are feasible is infinite nuclear matter. The calculation of the nuclear matter  $P(\mathbf{k}, E)$  within the orthogonal correlated-basis-function (CBF) perturbation theory, using a nuclear hamiltonian including two- and three-body interactions, is described in the work of Benhar et al. [10], and an application to inclusive electron scattering is reported in Ref. [11]. Theoretical studies of the nuclear-matter spectral function have been also carried out using different versions of the G-matrix perturbation theory and semirealistic nuclear hamiltonians [12–14]. The  $P(\mathbf{k}, E)$  resulting from these calculations exhibit the same qualitative behaviour of the spectral function as discussed in Ref. [10], but no applications to inclusive electron scattering are available.

The main drawback of nuclear-matter calculations is the limited set of data one can compare to. Only for a very few observables and kinematics are there sufficient data available to extrapolate from finite nuclei to nuclear matter (see the results of Day et al. [15,16]). For inclusive electron scattering the main limitations occur for very large  $q$ , where data are scarce, so that an extrapolation to nuclear

matter cannot be performed; a study of this region would be particularly interesting due to the sensitivity of the cross sections to short-range properties. It also has not yet been possible to extrapolate to nuclear matter the data separated into their longitudinal and transverse pieces; the extrapolation would lead to a further blowup of the uncertainties, which are already large. A study of the longitudinal response would be of interest in particular for a better understanding of the reaction mechanism and the elucidation of the difficulties encountered with the longitudinal sum rule.

In the present paper we derive an approximate  $P(\mathbf{k}, E)$  for the heavier nuclei. This will be done by combining the mean-field  $P(\mathbf{k}, E)$ , which is expected to be realistic at small  $k$  and  $E$ , with the correlation part extracted from the nuclear-matter calculation and recalculated for nuclei employing the local-density approximation (LDA).

For the case of the nuclear momentum distribution, the LDA has been used previously [17,18]. Stringari et al. started from the momentum distribution of nuclear matter calculated in lowest-order cluster approximation. For the application of the local-density approximation, they split the momentum distribution in a correlated and an uncorrelated piece, the latter being simply the momentum distribution of the noninteracting Fermi gas. The correlated part resulting from this procedure was  $< 0$  for  $k < k_F$ , and positive above  $k_F$ , and had vanishing normalization. The uncorrelated part and the density distribution needed for the application of the local-density approximation were calculated using the density-dependent Hartree–Fock (DDHF) approximation with a Skyrme interaction.

Co et al. [18] studied quantitatively the above LDA treatment with a fully consistent Fermi hypernetted-chain (FHNC) calculation carried out for a home-work NN interaction of the central type and Jastrow-correlated wave functions, for both nuclear matter and doubly-closed-shell nuclei.

The local-density approximation has also been applied by Pieper et al. [19] in a study of drops of liquid  ${}^4\text{He}$ . The results of Ref. [19] indicate that the pair-distribution function, describing the effect of short-range correlations on the two-body density, can successfully be approximated as a function of the local one-body density and the interparticle separation.

In the present work we develop an approach to split the nuclear-matter spectral function  $P(\mathbf{k}, E)$ , calculated for different nuclear-matter densities, into a correlated and a single-particle part. This is achieved by identifying in the calculation of  $P(\mathbf{k}, E)$  the contributions coming from configurations having pairs of strongly correlated nucleons, which are mostly sensitive to the short-range part of the NN interaction. These contributions are expected to be unaffected by finite-size effects, originating from long-range interactions, and can be evaluated in infinite nuclear matter. The resulting correlated spectral function  $P_{\text{cor}}(\mathbf{k}, E)$  is positive both below and above  $k_F$ . As the finite-nucleus single-particle part we employ the spectral functions measured via  $(e, e'p)$  reactions. This provides a realistic distribution as a function of momentum and removal energy.

With this approach we need to apply the LDA to the short-range properties of the nucleus *only*. For these aspects, the LDA is expected to work reliably.

The approach taken in this paper intends to tackle at the same time a second problem which is related to the understanding of inclusive electron scattering at large  $q$ , the tool we use to check  $P(\mathbf{k}, E)$  at large  $k$  and  $E$ . The inclusive cross sections, although less sensitive than exclusive data, are significantly affected by the final-state interaction of the recoil nucleon. This FSI needs to be accounted for in order to extract from  $(e, e')$  quantitative information. For the study of short-range properties of nuclei, this final-state interaction must be understood in kinematics where the recoil-nucleon momentum is large, i.e. where a relativistic description is needed. The work of Benhar et al. [11] has provided a way to treat the final-state interaction in the large- $q$  regime for nuclear matter. Employing the local-density approximation, we extend this approach to the description of inclusive scattering from finite nuclei.

## 2. Spectral function of nuclear matter

The one-body Green functions of nuclear matter at saturation density  $\rho_{\text{NM}} = 0.16 \text{ fm}^{-3}$  have recently been calculated for the non-relativistic nuclear hamiltonian with the Urbana  $v_{14} + \text{TNI}$  interaction, using the orthogonal-correlated-basis-function (OCBF) theory [10]. The spectral function is proportional to the imaginary part of the Green function which describes the propagation of hole states and can be written in the form

$$P(\mathbf{k}, E) = \sum_N |\langle 0 | a_{\mathbf{k}}^\dagger | N^{A-1} \rangle|^2 \delta(E - E_N^{A-1} + E_0^A), \quad (1)$$

where  $a_{\mathbf{k}}^\dagger$  creates a nucleon with momentum  $\mathbf{k}$ ,  $|0\rangle$  represents the nuclear-matter ground state, with energy eigenvalue  $E_0^A$ , and  $|N^{A-1}\rangle$  are intermediate excited states of the  $(A-1)$ -particle systems with energy eigenvalues  $E_N^{A-1}$ .

One-hole (1h)  $|N=\mathbf{k}\rangle$  and two-hole-one-particle (2h1p)  $|N=\mathbf{h}_i \mathbf{h}_j \mathbf{p}_i\rangle$  intermediate states have been included in the calculation. This has been achieved using OCBF perturbation theory within the set of correlated states (CSs)

$$|n\rangle_{\text{CS}} = \frac{\mathcal{S} |\Phi_n\rangle}{\langle \Phi_n | \mathcal{S}^\dagger \mathcal{S} | \Phi_n \rangle^{1/2}}, \quad (2)$$

where  $|\Phi_n\rangle$  is the generic eigenstate of the Fermi gas hamiltonian,  $\mathcal{S}$  is a many-body correlation operator of the form  $\mathcal{S} = S \prod_{i < j} F(i, j)$ , and where the two-body correlation operator  $F(i, j)$  has the same structure as the NN interaction [10].

The CSs  $|n\rangle_{\text{CS}}$  are first orthogonalized (OCS), by using the procedure described in Ref. [20], which preserves, in the thermodynamical limit, the diagonal matrix elements between CSs. Then, standard Rayleigh–Schrödinger perturbation theory is used to express the eigenstates  $|n\rangle$  in terms of the OCSs  $|m\rangle_{\text{OCS}}$ . Any eigenstate  $|\mathbf{h}_1 \dots \mathbf{h}_n \mathbf{p}_1 \dots \mathbf{p}_m\rangle$  has a large overlap with the  $n$ -hole- $m$ -particle OCSs  $|\mathbf{h}_1 \dots \mathbf{h}_n \mathbf{p}_1 \dots \mathbf{p}_m\rangle_{\text{OCS}}$ , and so OCBF perturbation theory is rapidly converging.

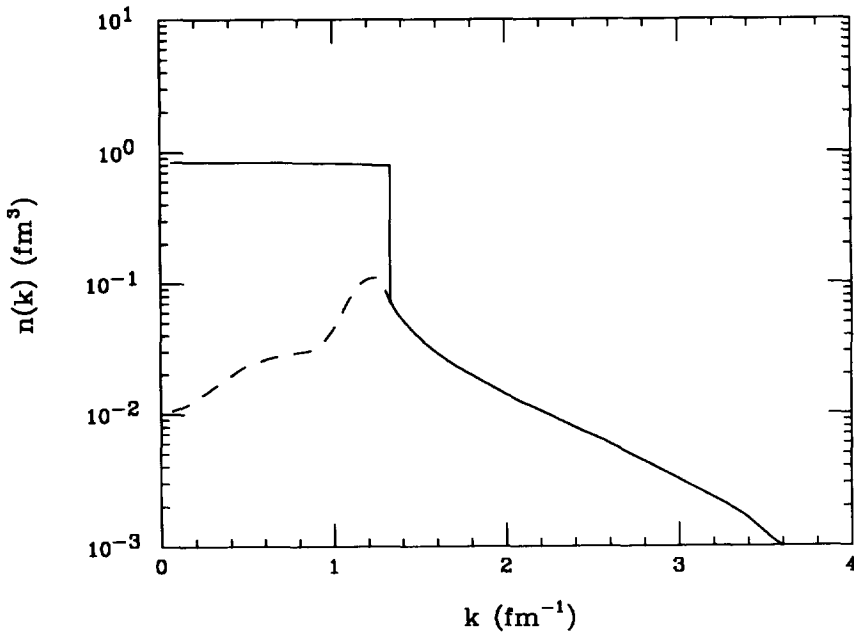


Fig. 1. Momentum distribution of nuclear matter at saturation density (full line). The dashed line represents the contribution associated with  $P_{\text{cor}}(k, E)$  for  $k < k_F$ .

The spectral function is most conveniently separated into two parts, according to its energy dependence: one part, which we will call *single-particle spectral function*  $P_{\text{s.p.}}(k, E)$ , corresponds to the contribution from 1h intermediate states and turns out to be sharply peaked at  $E = -e(k)$ ,  $e(k)$  being the excitation energy of the one-hole state  $|k\rangle$ . The width of the peak provides a measure of the lifetime of the hole state and goes to zero as it approaches the Fermi surface. The integral of  $P_{\text{s.p.}}(k, E)$  over the energy gives the strength  $Z(k)$  of the hole state, which is quenched with respect to unity [21], due to NN correlations.

The other part, denoted as *correlated spectral function*  $P_{\text{cor}}(k, E)$ , corresponds to contributions from  $n$ -hole- $(n-1)$ -particle states. It would be strictly zero in the absence of NN correlations and its leading contribution comes from 2h1p states. This part has a completely different energy dependence as compared to  $P_{\text{s.p.}}(k, E)$ , showing a widespread *background* extending up to large values of both  $k$  and  $E$ , with a maximum at  $E \sim k^2/2m$ .  $P_{\text{cor}}(k, E)$  coincides with  $P(k, E)$  for  $k > k_F$ . The integral of  $P_{\text{cor}}(k, E)$  over the energy gives the so-called continuous part of the momentum distribution  $n_c(k)$  [21], and the sum of  $n_c(k)$  with  $Z(k)$  provides the full momentum distribution, whose discontinuity at the Fermi surface is therefore given by  $Z(k_F)$ . The full nuclear-matter momentum distribution  $n(k)$ , and its continuous part  $n_c(k)$ , evaluated at the empirical saturation density, are shown in Fig. 1.

At the zeroth order of the OCBF perturbation theory, only diagrams with no internal *interaction points* (corresponding to non-diagonal matrix elements of the

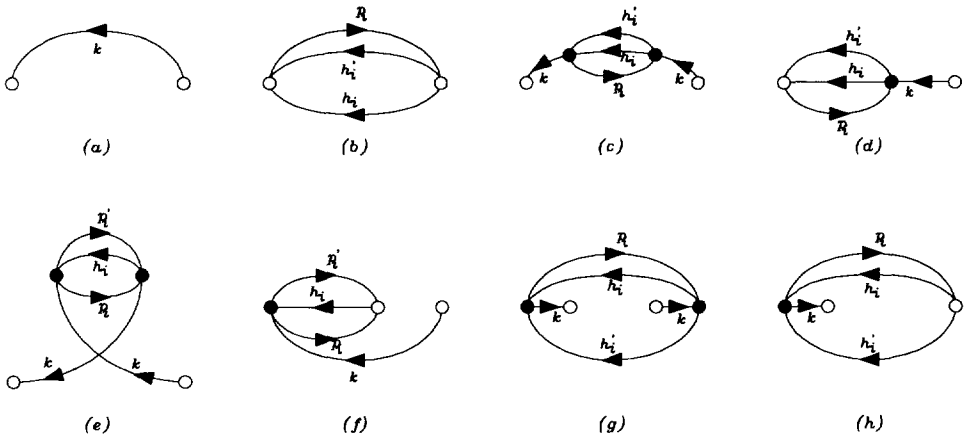


Fig. 2. Diagrams (a)–(h) as referred to in the text.

hamiltonian between OCSs and denoted as black dots in Fig. 2) are summed up. At this level, which we denote as *variational*, the separation of  $P(k, E)$  into  $P_{s.p.}(k, E)$  and  $P_{cor}(k, E)$  is straightforward. Diagram 2a represents the contribution from the 1h intermediate OCS, and contributes to  $P_{s.p.}(k, E)$ . Diagrams with  $n > 1$  hole lines and  $n - 1$  particle lines and no interaction points (diagram 2b shows the contribution from the 2h1p OCS) contribute to  $P_{cor}(k, E)$ .

Higher-order perturbative contributions  $\delta P(k, E)$  arise from corrections to the variational ground and intermediate states. These corrections are represented by OCBF diagrams with one or more interaction points. In these cases the separation into  $\delta P_{s.p.}$  and  $\delta P_{cor}$  may be more involved. However, it still can be readily performed for the corrections due to the admixtures of 2h2p states into  $|0\rangle$ : terms having  $|k\rangle_{OCS}$  as intermediate states belong to  $\delta P_{s.p.}$ , while those having all the remaining intermediate states contribute to  $\delta P_{cor}$ . Diagrams 2e and 2f are of the first type, whereas diagrams 2g and 2h are of the second one and vanish at  $k < k_F$ .

Each of the remaining diagrams contributes to both  $\delta P_{s.p.}$  and  $\delta P_{cor}$ . Let us analyze diagrams 2c and 2d. They derive from perturbative corrections to either the intermediate OCS state  $|k\rangle_{OCS}$  or to  $|h_i h_i p_i\rangle_{OCS}$ . The explicit expression of diagram 2d is

$$\delta P^{(2d)}(k, E) = \frac{1}{\pi} \text{Im} \left( \frac{\sum_{PO} (k, E)}{-e(k) - E - i\eta} \right), \tag{3}$$

where [10] the polarization self-energy  $\Sigma_2^{PO}(k, E)$ , at  $k < k_F$  and  $E > -e(k_F)$ , is given by

$$\sum_2^{PO} (k, E) = \frac{1}{2} \sum_{OCS} \frac{\langle 0 | a_k^\dagger | k \rangle_{OCS} \langle k | H | h_i h_i p_i \rangle_{OCS}}{e(p_i) - e(h_i) - e(h_i) - E - i\eta} + \text{c.c.} \tag{4}$$

It is clear from the above equations that two terms with different energy behaviour

are present: a  $\delta(e(k) + E)$  energy-dependent part, related to  $|\mathbf{k}\rangle$  and contributing to  $\delta P_{s,p}$ , and a second term, coming from  $\text{Im}[\Sigma_2^{\text{PO}}(\mathbf{k}, E)]$ , and spread out in energy, which is in turn related to  $|\mathbf{h}_i \mathbf{h}_i' \mathbf{p}_i\rangle$  and contributes to  $\delta P_{\text{cor}}$ . This last piece is the analytical continuation, at  $k < k_F$ , of diagram 2h. A similar relationship holds for diagram 2c and its counterpart 2g. This is indeed a general behaviour, leading to the property that  $\delta P_{\text{cor}}(\mathbf{k}, E)$  is a continuous function at  $k = k_F$ .

$P_{\text{cor}}(\mathbf{k}, E)$  provides only a small fraction of  $P(\mathbf{k}, E)$  at  $k < k_F$ , so we have not carried out the complete calculation of  $\delta P_{\text{cor}}(\mathbf{k}, E)$ . We have used, instead, the following procedure to estimate it: the contribution  $\delta P_{\text{cor}}^{(1)}$ , from diagram 2d and from all those diagrams obtained by renormalizing its hole line (and which can be shown to be dominant at large energies), has been evaluated from

$$\begin{aligned} \delta P_{\text{cor}}^{(1)}(\mathbf{k}, E) = & \frac{1}{\pi} \text{Im} \left[ \sum_2^{\text{PO}}(\mathbf{k}, E) \right] \text{Re} \left\{ \alpha(k) [-E - e(k)] - \delta e_2(k) \right. \\ & - \text{Re} \left[ \sum_1^{\text{PO}}(\mathbf{k}, E) \right] + \text{Re} \left[ \sum_1^{\text{PO}}(\mathbf{k}, -e(k)) \right] \\ & \left. - i \text{Im} \left[ \sum_1^{\text{PO}}(\mathbf{k}, E) \right] \right\}^{-1}, \end{aligned} \tag{5}$$

where  $\alpha(k)$  and  $\delta e_2(k)$  can be found in Ref. [10], and  $\Sigma_1^{\text{PO}}(\mathbf{k}, E)$ , at  $k < k_F$  and  $E > -e(k_F)$ , is given by

$$\sum_1^{\text{PO}}(\mathbf{k}, E) = \frac{1}{2} \sum \frac{|\text{OCS} \langle \mathbf{k} | H | \mathbf{h}_i \mathbf{h}_i' \mathbf{p}_i \rangle_{\text{OCS}}|^2}{e(p_i) - e(h_i) - e(h_i') - E - i\eta}. \tag{6}$$

The leading contribution to the remaining part is provided by diagram 2c, and it is approximated by scaling its counterterm  $\delta P_{\text{cor}}^{(2g)}$ , from diagram 2g, evaluated at  $k = k_F$ . The final expression for  $\delta P_{\text{cor}}$ , at  $k < k_F$ , is

$$\delta P_{\text{cor}}(\mathbf{k}, E) \approx \delta P_{\text{cor}}^{(1)}(\mathbf{k}, E) + \beta_k \delta P_{\text{cor}}^{(2g)}(k = k_F, E), \tag{7}$$

where  $\beta_k$  has been fixed to fulfil the continuity condition of  $\delta P_{\text{cor}}(\mathbf{k}, E)$  at  $k = k_F$  and the overall normalization. The integral over the energy of  $\delta P_{\text{cor}}$  yields  $-\delta Z^{\text{INT}}(k)$  of Ref. [21].

The correlated and single-particle contributions to the nuclear-matter spectral function at the empirical equilibrium density and  $k = 0.75k_F$  are shown in Fig. 3 together with the full  $P(\mathbf{k}, E)$  as a function of the removal energy  $E$ .

The density dependence of the nuclear-matter wave function and of the pair-distribution function has been studied by Wiringa et al. [22]. In the present work, we have computed the spectral function and the related sum rules at five different nuclear-matter densities, namely  $\rho = 1.25, 1.0, 0.75, 0.5$  and  $0.25 \rho_{\text{NM}}$ , using the Urbana  $v_{14} + \text{TNI}$  model of the NN interaction [23,24]. The corresponding momentum distributions are shown in Fig. 4. The results of these calculations confirm the naive expectation that the height of the quasiparticle peak increases when the density diminishes, whereas its width becomes smaller. The extension and importance of the background are much larger at higher densities. The

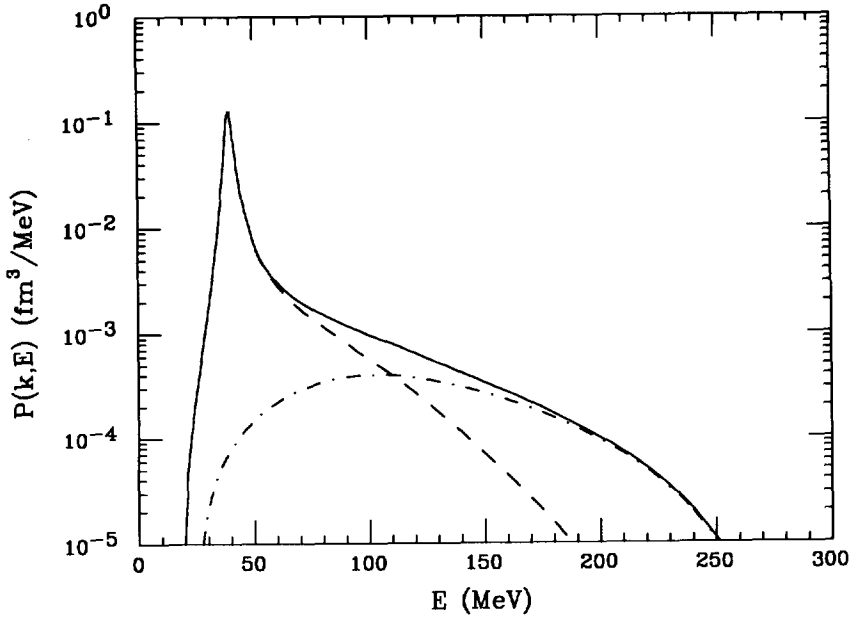


Fig. 3. Spectral function of nuclear matter at saturation density (full line) for  $k/k_F = 0.75$ . The dashed and the dash-dotted lines correspond to  $P_{sp}(k, E)$  and  $P_{cor}(k, E)$ , respectively.

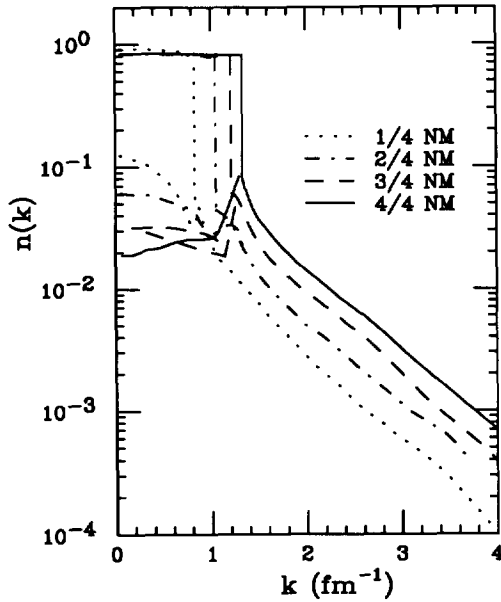


Fig. 4. Momentum distribution of nuclear matter at various densities. For each density the lower curve at  $k < k_F$  gives the contributions associated with the corresponding  $P_{cor}(k, E)$ .

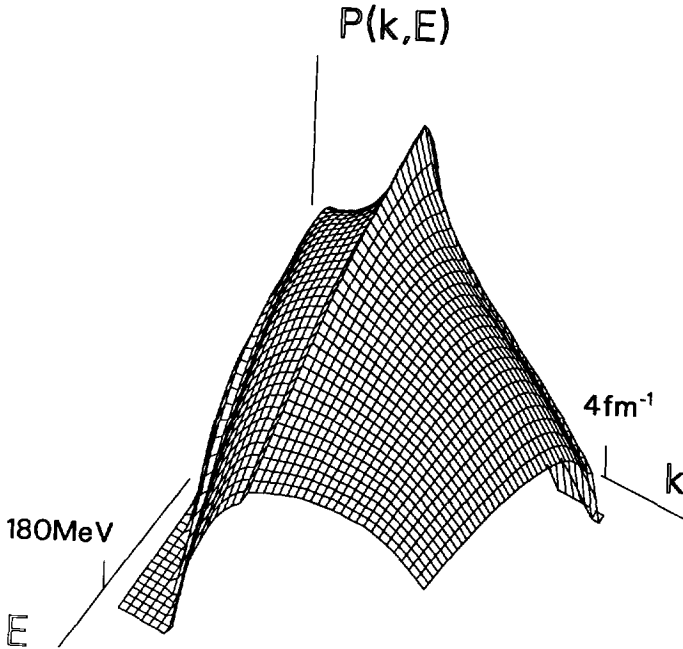


Fig. 5. Correlated part of  $P(k, E)$  (times  $k^2$ ) plotted as function of  $k$  and  $E$ , for  $\frac{3}{4}$  of the empirical nuclear-matter density.

calculated strengths of the quasi-hole pole at the Fermi surface,  $Z(e_F)$ , are  $Z(e_F) = 0.68, 0.68, 0.69, 0.61$  and  $0.60$  at  $\rho = 1.25, 1.0, 0.75, 0.5$  and  $0.25 \rho_{\text{NM}}$ , respectively. For a purely repulsive interaction, one would expect  $Z$  to approach unity for low densities; the attraction given by the empirical NN interaction is causing the correlation function to over-shoot 1, which simulates bound states of pairs of nucleons and explains why  $Z$  does not approach 1 for low density. The empirical information on the spectroscopic factor of the  $3s_{1/2}$  state in  $^{208}\text{Pb}$ , coming from  $(e, e)$  and  $(e, e'p)$  experiments, provides a value of  $0.65 \pm 0.05$  [25,26], in fair agreement with the OCBF estimate of  $Z(e_F)$  for nuclear matter of the appropriate density.

For illustration, we show in Fig. 5 a 3-dimensional plot of the correlated part of  $P(k, E)$ , calculated for  $\frac{3}{4}$  of the empirical nuclear-matter density. This plot clearly shows the enhancement of  $P(k, E)$  at large  $k$  and  $E$  due to short-range NN correlations.

### 3. Local-density approximation

#### 3.1. Spectral function

A generic two-body quantity  $F(1, 2)$  related to nuclear properties may be calculated within the local-density approximation (LDA) if its dependence on the

center-of-mass coordinate  $\mathbf{R} = \frac{1}{2}(\mathbf{r}_1 + \mathbf{r}_2)$  is weak. This is indeed the case for short-range functions having a range in the interparticle distance  $\mathbf{r} = \mathbf{r}_2 - \mathbf{r}_1$  which is small with respect to the surface thickness of the nucleus. In order to apply the LDA, the spectral function is better studied in the coordinate rather than in the momentum representation. The  $r$ -space spectral function is given by

$$P(\mathbf{r}_1, \mathbf{r}_1', E) = \sum_N \langle 0 | a^\dagger(\mathbf{r}_1) | N^{A-1} \rangle \langle N^{A-1} | a(\mathbf{r}_1') | 0 \rangle \delta(E - E_N^{A-1} + E_0^A), \quad (8)$$

and its integral over the energy gives the one-body density matrix

$$\rho(\mathbf{r}_1, \mathbf{r}_1') = \langle 0 | a^\dagger(\mathbf{r}_1) a(\mathbf{r}_1') | 0 \rangle = \int dE P(\mathbf{r}_1, \mathbf{r}_1', E). \quad (9)$$

Both the spectral function and the density matrix can be expressed in terms of the variables  $\mathbf{r}$  and  $\mathbf{R}$  instead of  $\mathbf{r}_1$  and  $\mathbf{r}_1'$ . The  $r$ -Fourier transform of  $P(\mathbf{R}, \mathbf{r}, E) \equiv P(\mathbf{r}_1, \mathbf{r}_1', E)$  is a measure [27] of the probability of removing a nucleon with a given momentum  $\mathbf{k}$  at a distance  $\mathbf{R}$  from the center of the nucleus associated with a removal energy  $E$ :

$$P(\mathbf{R}, \mathbf{k}, E) = \int d\mathbf{r} e^{i\mathbf{k} \cdot \mathbf{r}} P(\mathbf{R}, \mathbf{r}, E). \quad (10)$$

Integration of  $P(\mathbf{R}, \mathbf{k}, E)$  over  $\mathbf{R}$  gives the spectral function  $P(\mathbf{k}, E)$  defined previously,

$$P(\mathbf{k}, E) = \int d\mathbf{R} P(\mathbf{R}, \mathbf{k}, E). \quad (11)$$

As discussed in the preceding section for the nuclear-matter spectral function,  $P(\mathbf{R}, \mathbf{r}, E)$  can be separated into a single-particle part and a correlated one,

$$P(\mathbf{R}, \mathbf{r}, E) = P_{\text{s.p.}}(\mathbf{R}, \mathbf{r}, E) + P_{\text{cor.}}(\mathbf{R}, \mathbf{r}, E), \quad (12)$$

where  $P_{\text{s.p.}}$  is obtained when only the one-hole correlated states are included in the sum of Eq. (8).

In the present work, the single-particle part  $P_{\text{s.p.}}$  for finite nuclei is obtained from the momentum dependence of the single-particle wave functions, as determined from  $(e, e'p)$  reactions [28]. This leads to the mean-field spectral function

$$P^{\text{MF}}(\mathbf{r}_1, \mathbf{r}_1', E) = \sum_\alpha \phi_\alpha^*(1) \phi_\alpha(1') \delta(E - E_\alpha), \quad (13)$$

where the single-particle wave functions  $\phi_\alpha$  are extracted from the measured single-particle momentum distributions [29]. To account for the quenching of the single-particle states due to NN short-range correlations we have normalized the mean-field spectral function to the average strength factor  $Z$  taken from the nuclear-matter calculations as discussed in the preceding section:

$$P_{\text{s.p.}}(\mathbf{R}, \mathbf{r}, E) \sim Z^{\text{NM}}(\rho(\mathbf{R}), e_F) P^{\text{MF}}(\mathbf{R}, \mathbf{r}, E), \quad (14)$$

where  $Z^{\text{NM}}(\rho(\mathbf{R}), e_{\text{F}})$  is the quasiparticle strength for nuclear matter at the Fermi energy and density  $\rho(\mathbf{R})$ . Within the approximation employed here,  $P_{\text{s.p.}}(\mathbf{k}, E)$  has a  $\delta$ -function dependence on the energy  $E$ . The width of the single-particle peak, due to the decay of one-hole correlated states into the other CBF states, could easily be taken into account by using the full experimental  $E$ -dependence. However, such an improvement is not necessary here, because the calculation of the inclusive cross section involves an integration over  $E$ ; moreover, the data to be compared with have an energy resolution of  $\sim 30$  MeV. For the same reason, we neglect the effect of long-range correlations (beyond the ones already accounted for by the  $(e, e'p)$  results) as they would lead to a redistribution of the strength over a narrow interval in  $E$ .

We also neglect the fact that the occupation of the single-particle orbits could have a dependence on the orbit; the  $(e, e'p)$  results [28] indicate that this dependence is quite weak.

Alternatively we could have used mean-field calculations such as DDHF to determine the momentum distributions. We would expect to find very similar results, as the mean-field calculations are quite successful in reproducing the experimental momentum distributions measured at low  $k$  by  $(e, e'p)$ .

The correlated part  $P_{\text{cor}}(\mathbf{R}, \mathbf{r}, E)$  for finite nuclei has been calculated by using LDA. The cluster diagrams corresponding to  $\rho_{\text{cor}}(\mathbf{R}, \mathbf{r}) \equiv \rho_{\text{cor}}(\mathbf{r}_1, \mathbf{r}_1')$  have the two external points 1 and 1' linked by dynamical correlations; thus  $\rho_{\text{cor}}(\mathbf{R}, \mathbf{r})$  is short-ranged in  $\mathbf{r}$ . Therefore, it is plausible to use LDA to evaluate it. The approximation

$$\rho_{\text{cor}}(\mathbf{R}, \mathbf{r}) \sim \rho(\mathbf{R})\rho_{\text{cor}}^{\text{NM}}(\rho(\mathbf{R}), \mathbf{r}), \tag{15}$$

where  $\rho^{\text{NM}}$  is normalized so that  $\rho^{\text{NM}}(r=0) = 1$ , relies on the feature that the exchange correlation may be approximated by

$$\sum_{\alpha} \phi_{\alpha}^*(\mathbf{R} + \frac{1}{2}\mathbf{r})\phi_{\alpha}(\mathbf{R} - \frac{1}{2}\mathbf{r}) \sim \rho_0(\mathbf{R})l(k_{\text{F}}r), \tag{16}$$

for a range of  $r$ -values which is small with respect to the surface thickness of the nucleus. In the above equation  $l(k_{\text{F}}r)$  is the Fermi gas density matrix,  $k_{\text{F}} = (\frac{3}{2}\pi^2\rho_0)^{1/3}$  is the Fermi momentum, and

$$\rho_0(\mathbf{R}) = \sum_{\alpha} \phi_{\alpha}^*(\mathbf{R})\phi_{\alpha}(\mathbf{R}) \tag{17}$$

is the uncorrelated one-body density. A similar LDA has been recently analyzed in Ref. [18] for the case of Jastrow-correlated model nuclei, and found to provide extremely good results. We have verified that using  $\sqrt{\rho(\mathbf{r}_1)\rho(\mathbf{r}_1')}$  instead of  $\rho(\mathbf{R})$  in Eq. (15), as was done in Ref. [18], leads to almost indistinguishable results for the density matrices of the model nuclei considered in Ref. [18]. Here, we have adopted the simpler choice (15). As a consequence, we have used the following approximation for the correlated part of the  $r$ -space spectral function:

$$P_{\text{cor}}(\mathbf{R}, \mathbf{r}, E) \sim P_{\text{cor}}^{\text{LDA}}(\mathbf{R}, \mathbf{r}, E) = \rho(\mathbf{R})P_{\text{cor}}^{\text{NM}}(\rho(\mathbf{R}), \mathbf{r}, E). \tag{18}$$

### 3.2. Inclusive cross section

The inclusive electron–nucleus cross sections have been calculated following the approach developed in Ref. [11] for nuclear matter; here we extend this approach using LDA for the treatment of final-state interactions (FSI) in finite nuclei. In Born approximation the inclusive cross section is given by

$$\frac{d^2\sigma}{d\Omega d\epsilon'} = \frac{\alpha^2}{q^4} \frac{\epsilon'}{\epsilon} L^{\mu\nu} W_{\mu\nu}^A(q), \quad (19)$$

where  $\alpha = \frac{1}{137}$  is the fine-structure constant,  $\epsilon$  and  $\epsilon'$  are the energies of the incident and scattered electron, and  $q$  is the four-momentum transferred by the virtual photon:  $q \equiv k_e - k'_e$ , with  $k_e \equiv (\epsilon, \mathbf{k}_e)$  and  $k'_e \equiv (\epsilon', \mathbf{k}'_e)$ .  $L^{\mu\nu}$  and  $W_{\mu\nu}^A$  are the lepton and nuclear tensors, respectively.

The PWIA expression of the nuclear tensor is given by

$$W_{\mu\nu,IA}^A(q) = \int d\mathbf{R} \mathscr{W}_{\mu\nu,IA}^A(\mathbf{R}, q), \quad (20)$$

with

$$\mathscr{W}_{\mu\nu,IA}^A(\mathbf{R}, q) = \int d\mathbf{k} dE P(\mathbf{R}, \mathbf{k}, E) \left[ Z \tilde{W}_{\mu\nu}^p(\mathbf{k}, E, q) + N \tilde{W}_{\mu\nu}^n(\mathbf{k}, E, q) \right], \quad (21)$$

where  $\tilde{W}_{\mu\nu}^{p(n)}$  is the electromagnetic tensor of an off-shell proton (neutron), and its expression can be found in Ref. [11]. In the calculation of  $\mathscr{W}$  we employ the appropriate relativistic expressions as imposed by the high recoil-nucleon momenta.

Final-state interactions (FSI) have been included by using the convolution approximation and correlated Glauber theory (CGT), as developed in Ref. [11]. In this approach the effects of FSI appear in a quantity that is analogous to, but more complicated than, the usual optical potential  $V$ . The convolution approximation is a direct consequence of neglecting the dependence of the complex *potential*  $V = U + iW$ , felt by the struck nucleon in the nuclear medium, on the energy release  $\omega$  in the scattering process. This approximation has been successfully used in an number of studies of inclusive scattering on quantum liquids [30,31], and on nuclei [32].

According to the convolution approximation, the nuclear tensor is given by

$$W_{\mu\nu}^A(q) = \int d\mathbf{R} \int_0^\infty d\omega' F(\mathbf{R}, \mathbf{p}, \omega - \omega') \mathscr{W}_{\mu\nu,IA}^A(\mathbf{R}, |\mathbf{q}|, \omega'), \quad (22)$$

where  $\mathbf{p} = \mathbf{k} + \mathbf{q}$  is the momentum of the recoiling nucleon, and where the folding function  $F$  is given by

$$F(\mathbf{R}, \mathbf{p}, \omega - \omega') = \frac{1}{\pi} \text{Re} \left( \int_0^\infty dt \exp[i(\omega - \omega')t] e^{-iV(\mathbf{R}, \mathbf{p}, t)t} \right). \quad (23)$$

The folding accounts for the interaction of the knocked-out nucleon with the  $(A - 1)$ -particle system, which couples the initial  $1p1h$  state to more complicated  $2p2h$  states, etc.. Due to this, the initial  $1p1h$  state acquires a width and does not have to be on-shell. As a consequence the folding function  $F(\mathbf{R}, \mathbf{p}, \omega)$  extends to both negative and positive  $\omega$ -values. Similar features are present also in non-relativistic calculations of the longitudinal response carried out for lower momentum transfer [10], where FSI effects are “fully” included by means of OCBF theory.

Within CGT, the imaginary part of  $V$  is obtained from [11,33]

$$V(\mathbf{R}, \mathbf{p}; t) = -\frac{2\pi}{qt} \int_0^{v(p)t} d\xi \int \frac{d\mathbf{k} d\mathbf{r}}{(2\pi)^3} \sum_{\alpha=n,p} \rho(\mathbf{r}) f_p^{(N\alpha)}(\mathbf{k}) \times \exp[i\mathbf{k} \cdot (\mathbf{r} - \mathbf{R} - \hat{\mathbf{p}}\xi)] g(\mathbf{R}, \mathbf{r}), \quad (24)$$

where  $f_p^{(N\alpha)}(\mathbf{k})$  is the  $(N\alpha)$  amplitude for a nucleon of momentum  $\mathbf{p}$ .

At high momentum transfer, e.g.  $q^2 = 2$  to  $10$   $(\text{GeV}/c)^2$ , and for reactions on medium-heavy nuclei one can safely use LDA, approximating the pair function  $g(\mathbf{r}_1, \mathbf{r}_2)$  with the nuclear matter  $g^{\text{NM}}(\rho(\mathbf{R}), r_{12})$  and performing the amplitude average. This is justified as the scattered electron is sensitive only to the FSI of the recoil nucleon that occurs within a distance of order  $1/q$ , which is small. Under this approximation, the imaginary part  $W$  results to be

$$W(\mathbf{R}, \mathbf{p}; t) \rightarrow \frac{2\pi\rho(\mathbf{R})}{qt} \int_0^{v(p)t} d\xi \int \frac{d\mathbf{k} d\mathbf{r}}{(2\pi)^3} \times \exp[i\mathbf{k} \cdot (\mathbf{r} - \hat{\mathbf{p}}\xi)] g^{\text{NM}}(\rho(\mathbf{R}), r) \text{Im}[f_p(\mathbf{k})], \quad (25)$$

where  $f_p(\mathbf{k})$  is the free NN amplitude taken from experiment [34,35]. (We neglect the effect [36] of the change of the scattering amplitude off-shell, as too little is known about it.) This expression for  $W$  leads to a folding function  $F(\mathbf{R}, \mathbf{p}, \omega - \omega')$  which coincides with the nuclear-matter folding function evaluated at  $\rho_{\text{NM}} = \rho(\mathbf{R})$ .

We note that it is important to include the NN correlation function  $g(r - r')$ , i.e. to use the *correlated* Glauber theory. This accounts for the fact that a nucleon in the nucleus is surrounded by a correlation hole, and therefore the probability of a collision with one of the spectator particles during the first 2 fm of its trajectory as a recoil nucleon is reduced.

In principle, the real part  $U$  could be evaluated with the same approach as used for the imaginary part  $W$ , i.e. from Eq. (25) but with  $\text{Im}[f_p(\mathbf{k})]$  being replaced by  $\text{Re}[f_p(\mathbf{k})]$ . We note, however, that the real and the imaginary part of the optical potential quantitatively have very different effects, and describe different aspects of the FSI. The imaginary part  $W$  accounts for two-body scattering processes involving large momentum transfers, which lead to a strong damping of the motion of the recoiling particle, whereas the real part  $U$  produces a shift of its energy. The effect of the imaginary part is known to be dominant at large momentum. The real

part can only play a role at  $t \sim 0$ , when the attenuation associated with the imaginary part is weak due to the correlation hole surrounding the struck nucleon. It is therefore reasonable to neglect its time dependence. Due to the smallness of its effects, an approximate treatment is sufficient.

$U(\mathbf{R}, p)$  is taken from the optical potential of a nucleon in nuclear matter with density  $\rho(\mathbf{R})$  for  $p \leq 3 \text{ fm}^{-1}$ . In Ref. [11] the phenomenological Dirac optical model was used at larger momenta. However, the calculated  $U$  was positive for  $p > 3 \text{ fm}^{-1}$ , which is inconsistent with the correlated Glauber theory. Here, we use the Glauber theory for  $p > 3 \text{ fm}^{-1}$ .

In the calculation of the inclusive response, we also include the effect of colour transparency. Here *colour transparency* refers to the fact that scattering at large momentum transfer preferably selects nucleons in a ‘small’ configuration where the quarks are close together and the colour of the three valence quarks is well shielded, and the idea that such a Fock state of the nucleon has an interaction with other nucleons which is reduced in strength. In order to describe this predicted phenomenon, we have employed in our calculations a standard parametrization of the cross section [37], and the evolution of the ‘small’ Fock state back to the normal nucleon is treated as proposed by Ref. [38].

The ‘‘colour transparency’’ only plays a role for nucleons with initial momenta  $k < k_F$ , i.e. nucleons associated in PWIA with values of the Bjorken scaling variable  $X \approx 1$ . The FSI only produces large effects when moving the strength corresponding to initial momenta  $k < k_F$  to a lower energy loss, and it is only when FSI is large that colour transparency has an effect.

Different treatments of the FSI have been published by Nikolaev et al. and Kohama et al. [39,40]. Although these treatments refer to  $(e, e'p)$  rather than the inclusive cross section considered here, it may be instructive to compare to them.

For the description of correlations in the initial state, Nikolaev et al. use the independent pair approximation, with a parametrized distribution function. Their treatment of  $g(r_1 - r_2)$  does not include terms of order  $1/A$ , terms which are important to fulfill the normalization sum rule. Here, we use a fully correlated  $N$ -body wave function which takes into account consistently the many-body ground-state correlations; hence, the main contribution to FSI due to spectator nucleons is already included in our treatment. The remaining contributions coming from  $n$ -body distribution functions with  $n > 2$  correspond to the next order in our correlated Glauber theory, and are expected to be extremely small. In evaluating such contributions the use of the independent pair approximation as in Ref. [39] would largely overestimate the effect.

The treatment of FSI in  $(e, e'p)$  of Kohama et al. is similar to the correlated Glauber theory developed by Benhar et al. [11], but the NN correlations are introduced in a way similar to the one employed by Nikolaev et al.. With their parametrization of  $g$ , unrealistic at short distances as compared to the one obtained from microscopic calculations, they find smaller correlation effects than Benhar et al.. However, with a more realistic short-range behaviour, their correlation effects appear to double.

## 4. Results

### 4.1. Spectral function

In this section we want to discuss the numerical results obtained for  $P(\mathbf{k}, E)$ ,  $n(k)$  and the inclusive cross sections. We compare  $P(\mathbf{k}, E)$  and  $n(k)$  to the results of available microscopic calculations, and the calculated cross sections  $\sigma(q, \omega)$  to data on inclusive electron scattering.

For a calculation in terms of the local-density approximation discussed in the preceding section we need to treat separately the different regions of density of the nucleus, both in the calculation of  $P(\mathbf{k}, E)$  and in the calculation of the folding function  $F(\omega)$  which describes the effect of the FSI. As both  $P(\mathbf{k}, E)$  and  $F(\omega)$  are slowly varying functions of the density, it is sufficient to use a relatively coarse grid  $\zeta_i$  in densities.

In order to obtain the coefficients  $\nu_i$  that describe the fraction of the nucleus having density  $\zeta_i$  times the nuclear-matter density, we start from the charge density, known accurately from elastic electron scattering. We assume that proton and neutron densities have the same *shape*, and differ only by overall normalization ( $Z$  and  $N$ , respectively). The coefficients  $\nu_i$  are given by the fraction of nucleons located in the density bin centered at  $\zeta_i$  times the nuclear-matter density. For very light nuclei, we take into account the fact that the charge density is obtained from the nucleon density by folding with proton size. For the calculation of the  $\nu_i$  we use the unfolded density.

For the single-particle spectral function  $P_{\text{s.p.}}(\mathbf{k}, E)$ , we start from the momentum distributions of individual shells as determined from (e, e'p) reactions. The measured momentum distributions in general have been fitted with Woods–Saxon wave functions, which allows to easily recalculate  $P_{\text{s.p.}}(\mathbf{k}, E)$  (for a review see Frullani et al. [29]). For the case where the parametrization is given in radial space, we take the appropriate Fourier transform. The sum over all occupied shells gives the mean-field  $P_{\text{s.p.}}(\mathbf{k}, E)$ . Within the approximation employed here,  $P_{\text{s.p.}}(\mathbf{k}, E)$  corresponds to a sum of  $\delta$ -functions in the  $E$ -direction, as justified in the previous section.

Alternatively, we could have used for the mean-field part the results from realistic mean-field calculations, such as density-dependent Hartree–Fock (DDHF) calculations employing finite-range forces [41,42]. Such calculations are known to reproduce well the  $r$ -space densities, and can thus be expected to do well on the mean-field part of the momentum distribution. For the present use, the calculation of inclusive scattering cross sections, we would expect that such DDHF momentum distributions would have produced very similar results for  $\sigma(q, \omega)$ .

The Woods–Saxon momentum distributions become very small at momenta beyond 400 MeV/c. Ref. [19] showed that, for drops of liquid helium, the quasiparticle orbits do indeed have momentum distributions that fall very quickly at large  $k$ , and do not have the high-momentum tail that occurs for the continuum part of the spectral function.

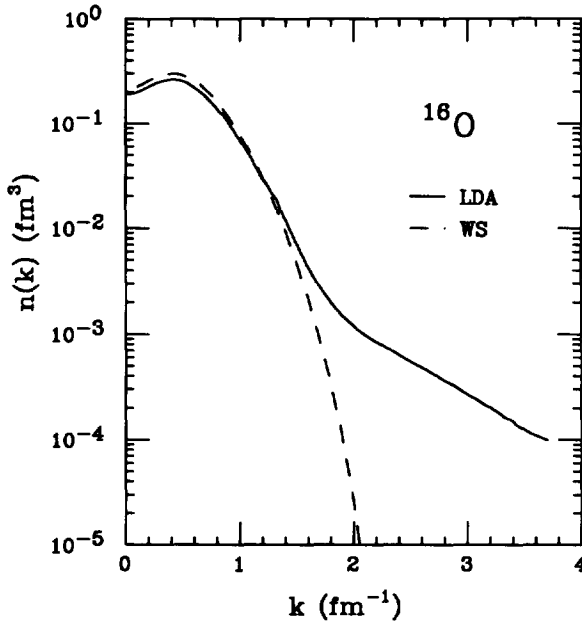


Fig. 6. Momentum distribution of oxygen in the local-density approximation (solid curve) and in the mean-field approximation (dashed curve).

For the correlated part  $P_{\text{cor}}(\mathbf{k}, E)$  we employ the spectral function of nuclear matter, calculated for different fractions  $\zeta_i$  of the full nuclear-matter density. The calculation of the nuclear-matter spectral function, and the relative normalization of the mean-field and correlated parts, have been discussed in the previous sections.

For a comparison between different approaches, we will limit ourselves to the confrontation of the momentum distributions  $n(k)$ , i.e. the spectral function  $P(\mathbf{k}, E)$  integrated over the removal energy  $E$ . A comparison of different results for  $P(\mathbf{k}, E)$  is not practical, and for most cases only calculations for  $n(k)$ , but not  $P(\mathbf{k}, E)$ , are available.

In Fig. 6 we show the momentum distribution for oxygen. The dashed curve gives the mean-field part, the full curve gives the sum of (renormalized) single-particle and correlated spectral functions. The effect of adding the short-range NN correlations is clearly visible in the tail at high  $k$ .

Fig. 7 gives a comparison of our momentum distribution (labeled LDA) and the one of Pieper et al. [9], calculated using the variational Monte Carlo (VMC) approach. This calculation was based on a realistic nucleon–nucleon potential, the Argonne  $v_{14}$  interaction supplemented by the Urbana VII three-nucleon potential. In spite of the fact that the two results have been obtained using different nuclear hamiltonians, we observe a remarkable agreement, indicating that the local-density approximation is likely to be a good approximation for the description of the correlated part. The small differences at low  $k$  probably reflect a shortcoming of

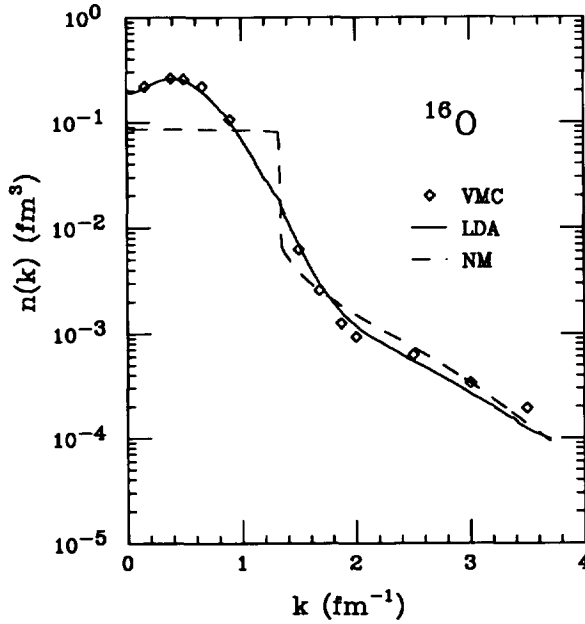


Fig. 7. Momentum distribution of oxygen: LDA (solid line), variational Monte Carlo calculation [9] (squares), nuclear-matter momentum distribution, normalized to 16 nucleons (dashed).

the variational wave function employed in Ref. [9], whereas the differences at large  $k$  come from both the statistical fluctuations of the VMC calculation and from the differences in the hamiltonians and in the correlation operators. For illustration, Fig. 7 also gives the  $n(k)$  of infinite nuclear matter.

We have also compared our results to the momentum distribution of VanOrden et al. [43] calculated using the RBHF approach and the Reid soft-core NN interaction. As the momentum distribution of VanOrden is nearly indistinguishable from the one calculated via VMC, we do not show it in Fig. 7.

In order to see just how far the LDA could be pushed, we have also applied it to  $^4\text{He}$ . Clearly,  $^4\text{He}$  is too small a nucleus to allow for a justifiable use of the LDA. The extrapolation of cross sections to nuclear matter performed by Day et al. [15] has also shown that  $^4\text{He}$  stands apart from the nuclei  $A \geq 12$  that allow – also within the local-density approximation – an extrapolation to nuclear matter. (While the data for  $A \geq 12$  defined a straight line as a function of  $A^{-1/3}$ , the data point for  $^4\text{He}$  deviated from it.) Surprisingly, however, the LDA does still extremely well for  $n(k)$  of  $^4\text{He}$ , as shown by Fig. 8. The momentum density obtained in the LDA is very close to the one of Schiavilla et al. calculated using the VMC approach [44]. We also compare in Fig. 8 to the momentum distribution obtained by Morita and Suzuki [4], who have calculated the  $^4\text{He}$  wave function using the ATMS approach and the Reid soft-core  $v_8$  interaction. The differences between the VMC and ATMS calculations are probably related to both the approximations

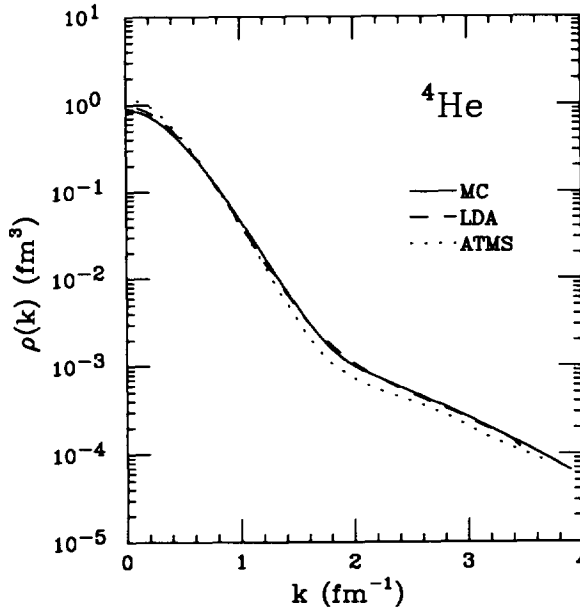


Fig. 8. Momentum distribution of  ${}^4\text{He}$ . LDA (dashed), Monte Carlo calculation [44] (solid), ATMS calculation [4] (dotted).

made in the latter calculation and to the NN interaction. While we do not advocate use of the LDA for  $A < 12$ , we note that the LDA seems indeed to be quite effective in treating *short-range* properties of the wave function.

#### 4.2. Inclusive cross sections

In order to test the calculated  $P(k, E)$ , we compare to the data on inclusive electron scattering at high  $q$ . The data in the wings of the quasi-elastic peak are sensitive to the high-momentum aspects of the nuclear wave function [8]. The wing at low energy loss  $\omega$  is accessible to experiment.

To calculate the inclusive cross sections for finite nuclei, we employ the approach we have developed for nuclear matter [11], and extended in the previous section. For every density, we use the corresponding  $P(k, E)$  to calculate the cross section in IA, employing the off-shell electron–nucleon cross section of deForest [45]. All processes involving excitation of the nucleon are calculated according to Ref. [11], employing the experimental response of the free nucleons. The folding function required for the treatment of the final-state interaction is calculated using CGT, starting from the experimental NN interaction and the NN correlation function  $g(r - r')$  obtained from CBF theory. The reduction of final-state interaction due to colour transparency is taken into account as discussed in Refs. [11,33]. The FSI is evaluated separately for the different regions of density of the nucleus.

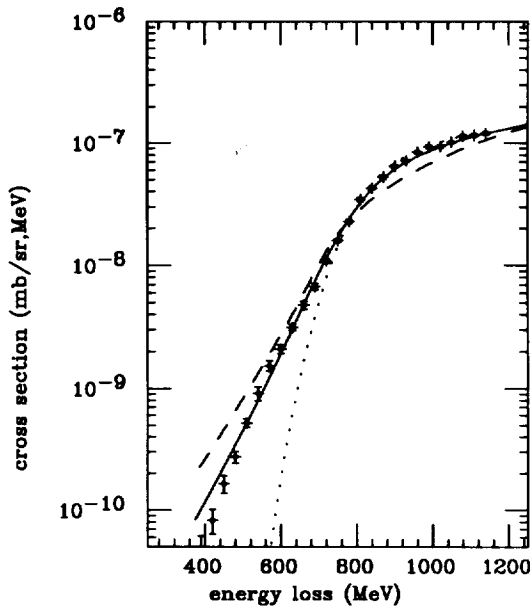


Fig. 9. Inclusive cross sections for  $^{12}\text{C}$  at 3.6 GeV and  $25^\circ$ . LDA result (full line), calculation employing the mean-field piece of the spectral function only and no FSI (dotted), calculation using the nuclear-matter spectral function and the corresponding FSI for the empirical nuclear-matter density (dashed).

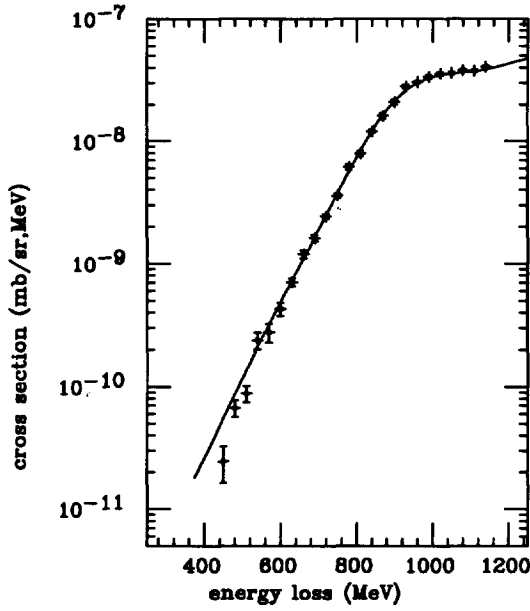
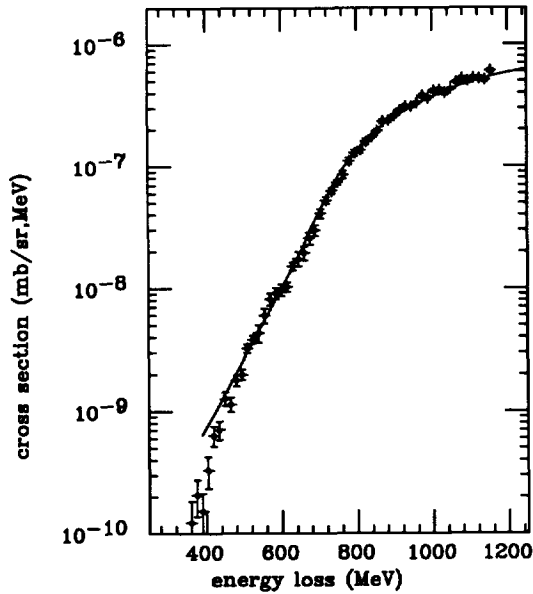
The effects of mesonic degrees of freedom in multi-nucleon processes, beyond the ones already included in  $P(k, E)$ , are neglected.

In Fig. 9 we show the cross sections for inclusive electron scattering from  $^{12}\text{C}$  at 3.6 GeV and  $25^\circ$ . The data are the ones of Day et al. [46,47]. The solid curve shows the full result, obtained using the spectral function calculated in local-density approximation, and the FSI treated in CGT. The calculation agrees very well with the data, both in the region of the quasi-elastic peak ( $\omega \approx 1$  GeV), and in the tail at small energy loss.

The dashed curve shown in Fig. 9 uses the nuclear-matter spectral function for the full nuclear-matter density, and the corresponding FSI. Due to the excess of high-momentum components, and a final-state interaction which is too strong, the cross section becomes too large at low energy loss. The dotted curve uses the mean-field part of the spectral function only, and no FSI (the long-range part of which has a small effect). This calculation also clearly disagrees with the data.

In Figs. 10 and 11 we show data and calculations for the same momentum transfer as in Fig. 9, but for  $^4\text{He}$  and  $^{56}\text{Fe}$ . Again we observe excellent agreement with the data. From this we conclude that the LDA allows to correctly treat the evolution of both the spectral function and final-state interaction as a function of  $A$ .

Fig. 12 shows for the same kinematics the iron data and calculation. While the dashed curve corresponds to the full calculation already discussed, the solid one is

Fig. 10. Inclusive cross sections for  ${}^4\text{He}$  at 3.6 GeV and 25°.Fig. 11. Inclusive cross sections for  ${}^{56}\text{Fe}$  for 3.6 GeV and 25°.

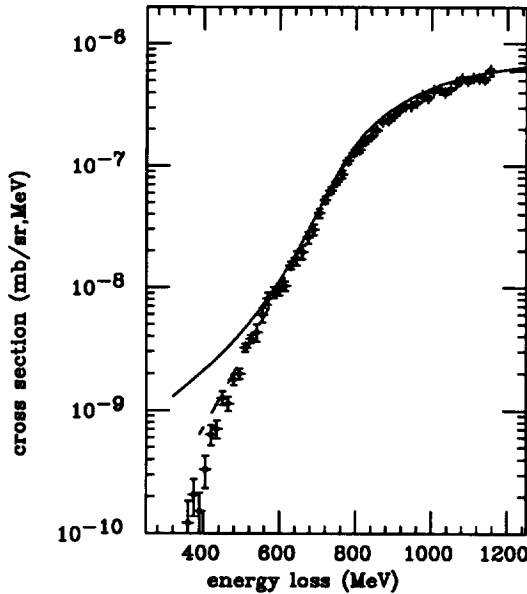


Fig. 12. Inclusive cross sections for  $^{56}\text{Fe}$  at 3.6 GeV and  $25^\circ$ . The LDA result (dashed line), without reduction of FSI due to colour transparency (solid line).

obtained by omitting the effect of colour transparency predicted to occur in QCD [38,48]. Fig. 12 shows that it is clearly important to include colour transparency, as it was the case for nuclear matter [11]. For  $^{56}\text{Fe}$  the effects of colour transparency are smaller, as has to be expected given the smaller average density of the matter the nucleon recoils into.

As a matter of fact, the effect of colour transparency is still appreciable, and much larger than for  $(e, e'p)$  at the same momentum transfer. This finding, which at first sight is somewhat counter-intuitive, is explained by the fact that in *inclusive* scattering one does observe the *full* effect of colour transparency, as  $1/q$ , the distance over which  $(e, e')$  is sensitive to the interaction of the recoiling system, is smaller than the distance within which the ‘small’  $3q$ -state evolves back to a normal nucleon. For  $(e, e'p)$ , the ‘standard’ tool considered for the study of colour transparency, a much larger  $q$  is needed to observe the full effect of colour transparency; to be specific,  $q$  has to be large enough to increase (by time dilatation) the lifetime of the “small state” to the time it takes to traverse the *entire nucleus*.

In Figs. 13 and 14 we further illustrate the quality of the results obtained. At the lower momentum transfers (Fig. 13) the agreement with data deteriorates somewhat at very low energy loss. The differences to experiment are very similar to the ones that had been observed for nuclear matter. These differences are the consequence of the decreasing accuracy of Glauber theory at the lower recoil-nucleon momenta. The folding function used for the description of FSI consequently is no longer as realistic as at higher nucleon momenta.

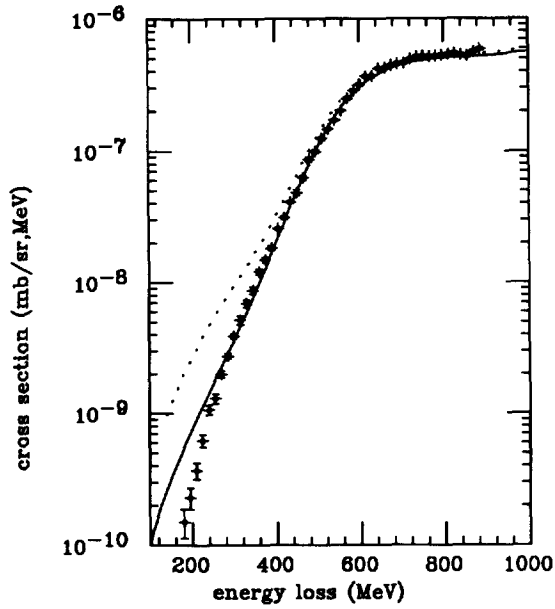


Fig. 13. Inclusive cross sections for  $^{12}\text{C}$  for 3.6 GeV and  $20^\circ$ . The dotted curve is obtained when neglecting the  $E$ -dependence of the spectral function.

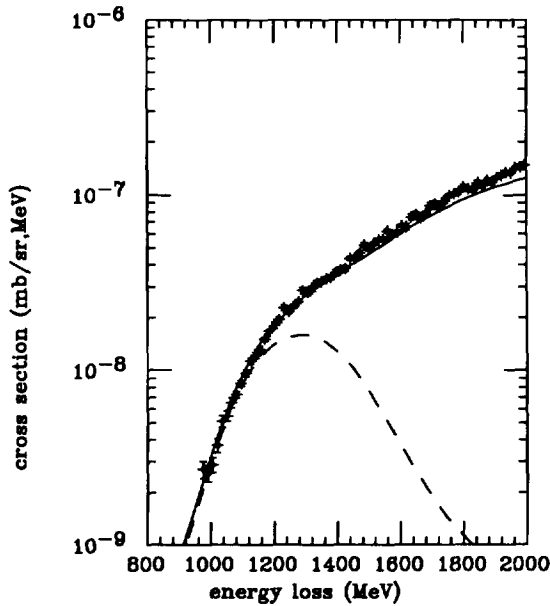


Fig. 14. Inclusive cross sections for  $^{12}\text{C}$  for 3.6 GeV and  $30^\circ$ . The dashed curve gives the quasi-elastic contribution alone.

In Fig. 13 we also illustrate that it is important to use in the calculation the full spectral function; with the often-used approximation of replacing  $P(\mathbf{k}, E)$  by the momentum distribution, the cross section is much too high at low  $\omega$  (dotted curve).

As shown by Fig. 14, the agreement with the data at higher momentum transfers remains very good; the quasi-elastic contribution (dashed line) increasingly becomes smaller relative to the large contribution of inelastic scattering on the nucleon at the larger  $\omega$ .

## 5. Conclusion

In the present work we address the problem of deriving a spectral function  $P(\mathbf{k}, E)$  for finite nuclei that is realistic at both low *and* high nucleon momenta, and small *and* large nucleon removal energies. As exact calculations for  $4 < A < \infty$  are not yet feasible, we employ an approach where we split the  $P(\mathbf{k}, E)$  into its single-particle and its correlated parts. The single-particle piece can be calculated using standard mean-field approaches such as DDHF with finite-range effective forces; alternatively it can be obtained from presently available data on  $(e, e'p)$  reactions. The correlated part can be calculated for nuclear matter for various nuclear-matter densities using CBF theory and a realistic NN interaction. As the correlated part concerns *short-range* nuclear properties only, the local-density approximation can be used to calculate the correlated part for finite nuclei.

We find that the resulting  $P(\mathbf{k}, E)$  agrees extremely well with the momentum distribution for those cases where variational Monte Carlo calculations can be performed. This is true even for a nucleus as light as  ${}^4\text{He}$ , where the LDA could no longer be expected to be applicable.

We use the resulting  $P(\mathbf{k}, E)$  to calculate the response for inclusive electron–nucleus scattering at large momentum transfer, a process that is sensitive to the high-momentum aspects of  $P(\mathbf{k}, E)$ . To achieve a quantitative description of  $(e, e')$  we also properly account for the short-range part of the recoil-nucleon final-state interaction. This again has become possible by using the LDA, without using any adjustable parameters.

We find excellent agreement between calculation and data for finite nuclei, similar in quality to the results previously obtained for infinite nuclear matter.

## Acknowledgements

The authors would like to thank V.R. Pandharipande for useful discussions. This work was supported by NSF grant PHY89-21025, and the Schweizerische Nationalfonds.

## References

- [1] A.E.L. Dieperink, T. de Forest, I. Sick and R.A. Brandenburg, *Phys. Lett. B* 63 (1976) 261
- [2] H. Meier-Hajduk, C. Hajduk, P.U. Sauer and W. Theis, *Nucl. Phys. A* 395 (1983) 332
- [3] C. Ciofi degli Atti, E. Pace and G. Salmè, *Phys. Rev. C* 21 (1980) 805
- [4] H. Morita and T. Suzuki, *Prog. Theor. Phys.* 86 (1991) 671
- [5] C. Ciofi degli Atti and S. Liuti, *Phys. Rev. C* 44 (1991) 1269
- [6] O. Benhar and V.R. Pandharipande, *Phys. Rev.* 47 (1993) 2218
- [7] I. Sick, Workshop on electron–nucleus scattering, eds. A. Fabrocini, S. Fantoni, S. Rosati and M. Viviani (World Scientific, Singapore, 1988) p. 552
- [8] I. Sick, D. Day and J.S. McCarthy, *Phys. Rev. Lett.* 45 (1980) 871
- [9] S.C. Pieper, R.B. Wiringa and V.R. Pandharipande, *Phys. Rev. C* 46 (1992) 1741
- [10] O. Benhar, A. Fabrocini and S. Fantoni, *Nucl. Phys. A* 505 (1989) 267
- [11] O. Benhar, A. Fabrocini, S. Fantoni, G.A. Miller, V.R. Pandharipande and I. Sick, *Phys. Rev. C* 44 (1991) 2328
- [12] C. Mahaux and C. Sartor, *Nucl. Phys.* 20 (1991) 1
- [13] A. Ramos, A. Polls and W.H. Dickhoff, *Nucl. Phys. A* 503 (1989) 1
- [14] H.S. Kohler, *Nucl. Phys. A* 537 (1992) 64
- [15] D. Day, J.S. McCarthy, Z.E. Meziani, R. Minehart, R.M. Sealock, S. Thornton, J. Jourdan, I. Sick, B.W. Filippone, R.D. McKeown, R.G. Milner, D. Potterveld and Z. Szalata, *Phys. Rev. C* 40 (1989) 1011
- [16] D. Day and I. Sick, *Phys. Lett. B* 274 (1992) 16
- [17] S. Stringari, M. Traini and O. Bohigas, *Nucl. Phys. A* 516 (1990) 33
- [18] G. Co, A. Fabrocini and S. Fantoni, *Nucl. Phys. A* (1993), in print
- [19] S.C. Pieper, R.B. Wiringa and V.R. Pandharipande, *Phys. Rev. B* 32 (1985) 3341
- [20] S. Fantoni and V.R. Pandharipande, *Phys. Rev. C* 37 (1988) 1697
- [21] O. Benhar, A. Fabrocini and S. Fantoni, *Phys. Rev. C* 41 (1990) 24
- [22] R.B. Wiringa, V. Fiks and A. Fabrocini, *Phys. Rev. C* 38 (1988) 1010
- [23] I.E. Lagaris and V.R. Pandharipande, *Nucl. Phys. A* 359 (1981) 331
- [24] I.E. Lagaris and V.R. Pandharipande, *Nucl. Phys. A* 359 (1981) 349
- [25] I. Sick and P. de Witt, *Comm. Nucl. Part. Phys.* 20 (1991) 177
- [26] L. Lapikás, *Nucl. Phys. A* 553 (1993) 297c
- [27] E. Wigner, *Phys. Rev.* 40 (1932) 749
- [28] P. deWitt Huberts, *J. of Phys. G* 16 (1990) 507
- [29] S. Frullani and J. Mougey, *Adv. Nucl. Phys.* 14 (1984) 1
- [30] L.J. Rodriguez, H.A. Gersch and H.A. Mook, *Phys. Rev. A* 9 (1974) 2085
- [31] R. Silver, *Phys. Rev. B* 38 (1988) 2283
- [32] Y. Horikawa, F. Lenz and N.C. Mukhopadhyay, *Phys. Rev. C* 22 (1980) 1680
- [33] O. Benhar, A. Fabrocini, S. Fantoni, V.R. Pandharipande and I. Sick, *Phys. Rev. Lett.* 69 (1992) 881
- [34] A.V. Dobrovolsky, A.V. Khanzadeev, G.A. Korolev, E.M. Maev, V.I. Medvedev, G.L. Sokolov, N.K. Terentyev, Y. Terrien, G.N. Velichko, A.A. Vorobyov and Yu.K. Zalite, *Nucl. Phys. B* 214 (1983) 1
- [35] B.H. Silverman, J.C. Lugol, J. Saudinos, Y. Terrien, F. Wellers, A.V. Dobrovolsky, A.V. Khanzadeev, G.A. Korolev, G.E. Petrov and A.A. Vorobyov, *Nucl. Phys. A* 499 (1989) 763
- [36] T. Uchiyama, A.E.L. Dieperink and O. Scholten, *Phys. Lett. B* 233 (1989) 31
- [37] L.L. Frankfurt and M.I. Strikman, *Phys. Reports* 160 (1988) 235
- [38] G.R. Farrar, H. Liu, L.L. Frankfurt and M.I. Strikman, *Phys. Rev. Lett.* 61 (1988) 686
- [39] N.N. Nikolaev, A. Szczurek, J. Speth, J. Wambach, B.G. Zakharov and V.R. Zoller, *Phys. Lett. B* 317 (1993) 281
- [40] A. Kohama, K. Yazaki and R. Seki, *Nucl. Phys. A* 551 (1993) 687
- [41] X. Campi and D.W.L. Sprung, *Nucl. Phys. A* 194 (1972) 401
- [42] D. Gogny, Nuclear self-consistent fields, eds. G. Ripka and M. Porneuf (North-Holland, Amsterdam, 1975)

- [43] J.W. VanOrden, W. Truex and M.K. Banerjee, *Phys. Rev. C* 21 (1980) 2628
- [44] R. Schiavilla, V.R. Pandharipande and R.B. Wiringa, *Nucl. Phys. A* 449 (1986) 219
- [45] T. de Forest, *Nucl. Phys. A* 392 (1983) 232
- [46] D. Day, J.S. McCarthy, Z.E. Meziani, R. Minehart, R. Sealock, S.T. Thornton, J. Jourdan, I. Sick, B.W. Filippone, R.D. McKeown, R.G. Milner, D.H. Potterveld and Z. Szalata, *Phys. Rev. Lett.* 59 (1987) 427
- [47] D. Day, J.S. McCarthy, Z.E. Meziani, R. Minehart, R. Sealock, S.T. Thornton, J. Jourdan, I. Sick, B.W. Filippone, R.D. McKeown, R.G. Milner, D.H. Potterveld and Z. Szalata, *Phys. Rev. C* 48 (1993) 1849
- [48] B.K. Jennings and G.A. Miller, *Phys. Rev. D* 44 (1991) 692